Research Article



Power sharing for transmission systems with 100% inverter-based generating resources

ISSN 1751-8687 Received on 31st March 2020 Revised 11th August 2020 Accepted on 22nd October 2020 E-First on 17th February 2021 doi: 10.1049/iet-gtd.2020.0610 www.ietdl.org

Saleh Ziaeinejad¹, Mohammad Mousavi¹, Ali Mehrizi-Sani² ⊠, Deepak Ramasubramanian³, Evangelos Farantatos³

¹Electrical Engineering and Computer Science, Washington State University, Pullman, WA, USA

Abstract: This study proposes controls and power sharing design and architecture for a 100% inverter-based transmission system. Such an operation scenario has already occurred for short periods in portions of several systems in the United States, Europe, and Australia, and is likely to be more frequent in the future. The proposed algorithm enables the inverter-based resources (IBR) to participate in power sharing based on an angle droop method that explicitly takes into account the IBR ratings and preferred set points. This strategy results in an essentially constant-frequency operation of the power system without relying on secondary controllers or communication for frequency restoration. The performance of the proposed architecture under different operating conditions is evaluated via extensive simulation case studies in PSCAD/EMTDC software.

1 Introduction

The electric power system, once dominated by traditional synchronous generation (SG), is experiencing a shift towards an increased share of power electronically (PE) interfaced generation [1-3]. This shift is mainly due to the increased integration of renewable energy resources, such as wind and photovoltaic (PV) solar [4], which use PE-based inverters, also known as inverterbased resources (IBR). For example, in the United States, the Bonneville Power Administration service area has several times experienced 100% wind generation at night; the ERCOT system had instances of 50% instantaneous penetration of wind. In Australia (Tasmania), the power system routinely experiences > 70% instantaneous inverter-based generation [2]. In Ireland, the operators are expected to accommodate up to 75% instantaneous inverter-based generation by 2020 [2]. A similar shift is being experienced in loads: electric drives, which employ an inverter interface for increased control and efficiency, are the largest consumer of electricity (about 64%) in the United States [4].

This shift towards inverter-based resources brings about significant challenges in power system dynamics, stability, and control [5, 6]. Most existing inverters are programmed to rigidly inject a certain value of power irrespective of the conditions of the grid. This mode of operation is termed grid following as the inverter synchronises to the grid voltage ('follows the grid') via a phase-locked loop (PLL) and normally operates as a controlled current source. However, the grid-following mode of operation is not adequate for an inverter-dominated power system (IDPS). This is because a PLL needs a relatively stiff voltage and frequency. While this requirement is normally met in a conventional SG-based power system, it may not be available in an IDPS. Therefore, some inverters may need to operate in a different mode to control the voltage and frequency of their buses. (In microgrid terminology, a similar objective is achieved using master and slave inverters [7-10].) Simultaneously, in an IDPS, it is imperative to ensure power sharing among all inverters. Power sharing is defined as coordinating dispatchable generation resources to meet the power demand under varying conditions.

In a conventional power system, power sharing is typically based on frequency droop, which stems from an SG's intrinsic relation between power (generation/load mismatch) and frequency (rotor speed) [11]. This power-frequency droop can also be adopted

for an IDPS via inverter controls. For example, the authors in [12, 13] discuss the control of inverters as a virtual SG, where the fundamental swing and electromechanical transient equations of an actual SG are implemented in the control logic. The advantage of this approach is that the IBR can use a similar controller as conventional SG-based units. Frequency droop may also be employed for a 100% inverter-based system. For example, in [14], the applicability of frequency droop to operate an all inverter North American interconnection is shown. Moreover, the European MIGRATE project [15] recently proposed an inverter control structure using the concept of threshold virtual impedance (TVI). TVI improves the transient behaviour of droop control; however, it needs a secondary controller to restore the frequency to its nominal value. To obviate the need for a secondary controller, Yazdanian and Mehrizi-Sani [16] proposed power sharing of inverters based on their frequency transients; however, it assumes a stiff grid and does not handle power sharing for inverters connected after the transient.

In general, frequency droop (i) is a steady-state concept and does not explicitly deal with fast transients including those of inverters and (ii) introduces a steady-state error in the frequency and needs a secondary controller to restore the frequency. In addition, in a 100% inverter-based system, the notion of frequency is relevant only for electrical quantities (rate of change of voltage angle), as there is no rotor to define mechanical frequency. Therefore, in such systems, the relevance and importance of frequency are not well-understood or -established. Based on this observation, Ramasubramanian *et al.* [17] proposed a constant-frequency operation paradigm based on angle droop [18] and discusses its reliability implications.

In angle droop, power sharing is achieved by changing the angle of the terminal voltage of the IBRs. The authors in [18–21] implemented angle droop for a parallel set of inverters connected to the same point of common coupling in a microgrid via a series filter. However, it needs central coordination and a communication link to assign reference angles to the inverters. In [22], angle droop is realised by an energy management system that monitors the power flows and determines the reference set points for real and reactive power of the IBRs. Again, this work is proposed for a microgrid. If the communication link fails, the controller reverts to frequency droop. In addition, the authors in [18–22] studied the

²Bradley Department of Electrical and Computer Engineering, Virginia Tech, Blacksburg, VA, USA

³Grid Operations and Planning Group, Electric Power Research Institute, Knoxville, TN, USA

[⊠] E-mail: mehrizi@vt.edu

Table 1 Comparison of the proposed angle droop method with other methods

with other methods				
Ref.	Angle	Applicable to	Require	Enforce
	droop		only	current and
				power
	method?	transmission	GPS to	limit of
		system?	operate?	inverters?
[16]	no	no	no	no
[18–23]	yes	no	no	no
[17, 24]	yes	yes	no	no
proposed method	yes	yes	yes	yes

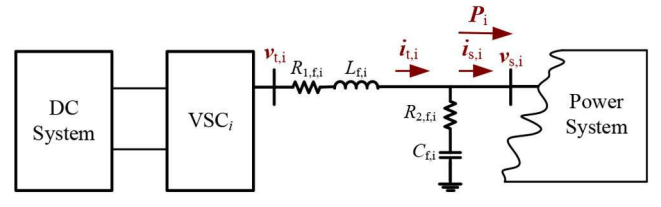


Fig. 1 Generation unit i, as an IBR, interfaced to the power system

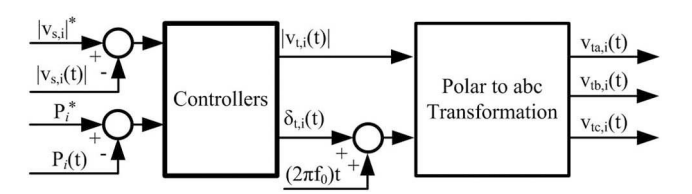


Fig. 2 Overall structure of the proposed controller

angle droop for microgrids, which all have a reference point for voltage angle of the system and can be calculated by local measurements. However, in the power system, there is no reference point for voltage angle. Thus, it cannot be measured through local measurements. Majumder *et al.* [23] proposed angle droop for a distribution system; however, it does not consider different modes of operation of inverters and their current and real power limits during both transient and steady-state operations. Therefore, studying and designing an angle droop-based controller for the power system merits more investigation.

In [17], the authors discussed the reliability implications of angle droop without an associated explicit communication link for nominal frequency operation. This paper builds on the proof of concept presented in [17, 24] and proposes a new power sharing algorithm that allows the inverters to deviate from their locally determined set points to participate in real power sharing once needed. The contributions of this paper are as follows:

- Propose a new angle droop-based power sharing algorithm for generation resources in a 100% inverter-based transmission power system that utilises only a global positioning system (GPS) and local signals and does not require wide-area communication.
- Augment the proposed algorithm with additional control mechanisms to enforce current and real power limits of inverters during both steady-state and transient operations.
- Propose a parameter design guideline for the proposed control and power sharing algorithm.

The proposed angle droop-based algorithm is compared with other methods in Table 1. The remainder of this paper is organised as follows. Section 2 presents the definitions and discusses inverter types. Section 3 discusses the proposed algorithms for the IBRs and provides insights into its operation principles. Section 4 discusses the parameter design for the proposed algorithms. Section 5 presents the simulation case studies to evaluate the performance of the proposed controller and power sharing method. The results show that the proposed method can regulate the voltage, real power, and frequency of the studied power system during load variations, dynamic loads, faults, and loss of GPS

signal, which confirms the performance of the proposed method. Concluding remarks are provided in Section 6.

2 Definitions

2.1 Inverter operation modes

Inverters employed in the power system, regardless of their hardware configuration, can operate in one of the two main modes: grid-following or grid-forming-roughly equivalent to slave and master controllers in the microgrid terminology [8]. The gridfollowing mode of the operation itself can be further divided into grid-parallel or grid-supporting modes. The output power of an inverter in the *grid-parallel* mode is agnostic to the grid conditions. A generation unit that uses a grid-parallel inverter is normally a non-dispatchable unit, e.g. a rooftop PV unit or wind turbine operating in maximum power point tracking mode. However, an inverter in the grid-supporting mode is dispatchable and can respond to the grid commands, e.g. by changing its injected real (and possibly reactive) power, to participate in power sharing. Both these modes normally operate the inverter as a controlled current source and synchronise to the grid using a PLL that follows the grid voltage—hence the name grid following. Thus, they need a stiff grid voltage and frequency, which may not be available in an inverter-dominated power system. (A grid-supporting inverter may also operate without a PLL or stiff voltage if angle information is provided through a GPS signal [25].)

In contrast, a *grid-forming* unit establishes and controls the grid voltage and frequency and is controlled as a voltage source. (Across the industry, there is yet no formally accepted definition for a grid forming inverter.)

2.2 Control objectives

Fig. 1 shows a generic grid-forming unit interfaced to the power system via an inverter [as a voltage-sourced converter (VSC)] and an resistor–inductor–capacitor filter with parameters R_{1,f_i} , L_{f_i} , R_{2,f_i} , and C_{f_i} . In this figure, i_{t_i} and i_{s_i} are the output current at the terminal of the VSC and the injected current to the power system, respectively.

The control objective of the inverter is to regulate its real power $P_i(t)$ and bus voltage magnitude $|v_{s,i}(t)|$ to their reference set points P_i^* and $|v_{s,i}|^*$. The instantaneous three-phase terminal voltages of the inverter $v_{i,i}(t)$ can be constructed via a modulation method by specifying its magnitude $|v_{i,i}(t)|$ and phase angle $\theta_{i,i}(t)$, whose reference points are determined by the proposed power sharing algorithm. Fig. 2 shows the overall structure of the associated controller. Section 3 discusses the details.

In a system at constant frequency f_0 , $\theta_{t,i}(t)$ is

$$\theta_{t,i}(t) = (2\pi f_0)t + \delta_{t,i}(t), \tag{1}$$

where $\delta_{t,i}(t)$ is referred to the voltage angle of the generation unit. As discussed below, in the proposed architecture, inverter units receive time t from GPS to be able to participate in angle droop. Modern power systems already use GPS data for measurement and control [19, 25, 26]. In addition, the proposed control algorithm can use an internal clock instead of GPS; however, whenever GPS is available and its integrity is verified, GPS time is used for synchronisation of the internal clocks. Thus, the dependency of the proposed controller to GPS data is only for the internal clock synchronisation, and the proposed algorithm is able to regulate the real power and voltage at their reference values even with the loss of GPS signal.

3 Proposed architecture for inverter-based resources

3.1 Proposed voltage magnitude controller

Fig. 3 shows the proposed voltage magnitude controller. When the selector is in +1 state, the controller uses an integral controller with gain G_1 to determine the inverter terminal voltage $|v_{i,i}(t)|$.

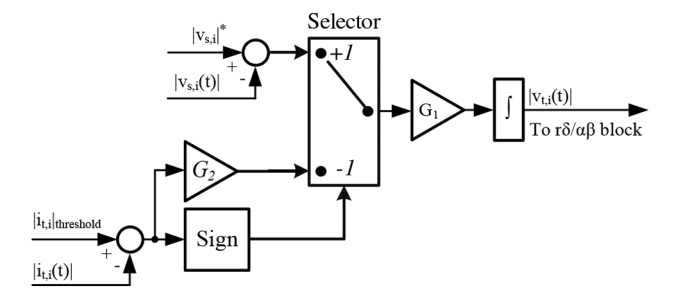


Fig. 3 Proposed voltage magnitude controller and current limiter

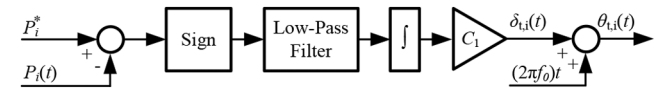


Fig. 4 Proposed real power controller

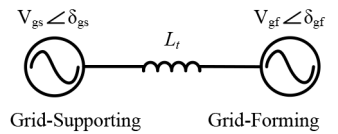


Fig. 5 A sample two-bus system

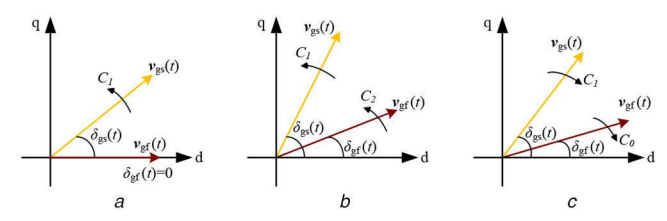


Fig. 6 Vector diagrams of the two-bus system under operating conditions (a) Grid-forming unit is large (see text for definition), (b) Grid-forming unit is limited, (c) Grid-forming unit is limited and brings δ_{eff} to zero

However, if current magnitude $|i_{i,i}(t)|$ exceeds its limit $|i_{i,i}(t)|_{\text{threshold}}$, the selector switches to -1 state, and the controller decreases the inverter terminal voltage with the gain G_1G_2 until it limits $|i_{i,i}(t)|$.

3.2 Proposed real power-sharing algorithm

The underlying idea behind the proposed real power sharing algorithm is that the injected real power of a generating unit at transmission levels can be controlled by adjusting its voltage angle. It is assumed that each grid-supporting unit has a preferred real power set point $P_{\rm gs}^*$ that depends on factors such as required power reserve, available power, and possibly operator commands. The proposed algorithm needs to ensure that the allocation of power to grid-forming and grid-supporting units can meet the total load demand. It calculates the modified power set point for each grid-supporting unit as

$$P_{\rm gs,droop}^*(t) = P_{\rm gs}^* + \Delta P_{\rm gs}^*(t), \tag{2}$$

where $P_{\rm gs,droop}^*$ is the modified set point due to the droop and $\Delta P_{\rm gs}^*$ is its adjustment (Section 3.3). The sum of these adjustments should equal the difference between the total demand and sum of the power supplied by the grid-forming unit and the preferred powers of the grid-supporting units

$$\sum \Delta P_{\rm gs,i}^* = P_{\rm demand} - P_{\rm gf} - \sum P_{\rm gs,i}^* = P_{\rm gs-total-change}, \tag{3}$$

where $P_{\rm gf} \leq P_{\rm gf,max}$. In our proposed power sharing algorithm, the following design principles are considered:

• Principle 1: the power limits of all grid-forming and gridsupporting units should be respected.

- Principle 2: the reference set points of grid-supporting units should not deviate from the preferred set points unless needed to meet power demand.
- Principle 2*: the algorithm should also allow participation of grid-forming and grid-supporting units, irrespective of their preferred set points, in power sharing.
- Principle 3: the share of grid-supporting units in power sharing should be based on their droop characteristic.

If the grid-forming unit is large enough, the grid-supporting units continue to inject their preferred real powers $P_{\rm gs,i}^*$. The grid-forming unit's voltage angle $\delta_{\rm gr}(t)$ is maintained at zero and the angles $\delta_{\rm gs,i}(t)$ of grid-supporting units are ramped at the rate C_1 until $P_{\rm gs,i}(t)$ reaches $P_{\rm gs,i}^*$ as shown in Fig. 4.

However, if the grid-forming unit is not large enough or if its $P_{\rm gf,max}$ is artificially lowered to redispatch power, the gridsupporting units do need to participate in power sharing. First, the proposed power sharing algorithm is discussed for the two-bus system shown in Fig. 5, in which the power generated by one inverter is consumed by the other (e.g. an island with a PV unit and a battery unit) and then extend it to a generic power system. In Fig. 5, the system has a transmission line with inductance $L_{\rm t}$. For simplicity, we assume a steady-state in which $\delta_{\rm gf}=0$; then the gridsupporting unit increases its power output to $P_{\rm gs}^*$. To meet $P_{\rm gs}^*$ similar to the previous case, the controller of the grid-supporting unit ramps its angle $\delta_{gs}(t)$ at the rate C_1 . Simultaneously, the gridforming unit compares its output power with the limit $|P_{\text{gf},\text{max}}|$. If $|P_{\rm gs}^*| < |P_{\rm (gf),max}|$, there is the same controls as the large grid-forming case discussed above. Fig. 6a shows the vector diagram for this operating condition in the dq frame synchronised to $(2\pi f_0)t$.

However, if $|P_{gs}^*| > |P_{(gf),max}|$, i.e. the power by the gridsupporting unit exceeds the capability of the grid-forming unit, as soon as $|P_{\rm gf}(t)| > |P_{\rm (gf),max}|$, the controller of the grid-forming unit changes its angle $\delta_{\rm gf}(t)$ to avoid further increase of its power and violating the limit. Fig. 6b shows the vector diagram for this operating condition. If $\delta_{gf}(t)$ is ramped at a rate $C_2 > C_1$, $\delta_{\rm gs}(t) - \delta_{\rm gf}(t)$ changes at the rate $C_1 - C_2$ until $|P_{\rm gf}(t)| = |P_{\rm gs}(t)| = |P_{\rm (gf),max}|$. Then the controller of the gridsupporting unit continues to ramp up $\delta_{gs}(t)$, but it cannot regulate $P_{\rm gs}(t)$ to $P_{\rm gs}^*$ because $\delta_{\rm gs}(t) - \delta_{\rm gf}(t)$ is influenced by the grid-forming unit and $C_2 > C_1$. As a result, the grid-supporting unit continuously rotates $v_{gs}(t)$ vector in the dq frame at a rotating speed of C_1 rad/s. Meanwhile, the grid-forming unit limits its power by rotating $v_{gf}(t)$ vector. Since $|P_{gf}(t)|$ changes around $|P_{(gf),max}|$, $v_{gf}(t)$ rotates in a stopand-move manner: It increases at a speed of C_2 rad/s whenever $|P_{\rm gf}(t)| > |P_{\rm (gf),max}|$ and stops whenever $|P_{\rm gf}(t)| \le |P_{\rm (gf),max}|$. The average speed of $v_{gf}(t)$ equals that of $v_{gs}(t)$ (i.e. C_1 rad/s). Therefore, the system frequency f_{sys} changes such that

$$|f_{\text{sys}} - f_0| = \frac{C_1}{2\pi}.$$
 (4)

both $v_{gf}(t)$ and $v_{gs}(t)$ vectors rotate in the dq frame at a speed of C_1 rad/s. Therefore, the system frequency f_{sys} changes such that

$$|f_{\text{sys}} - f_0| = \frac{C_1}{2\pi}.$$
 (5)

Eventually, $|P_{\rm gs}^*| < |P_{\rm [gf],max}|$, at which point it is preferred to bring $\delta_{\rm gf}(t)$ back to zero (at a rate C_0) to facilitate the implementation of the proposed angle droop algorithm presented in the next subsection.

However, changing $\delta_{\rm gf}(t)$ should not affect the ability of the grid-supporting unit to control its power $P_{\rm gs}(t)$. Therefore, C_0 should be smaller than C_1 so that while the grid-forming unit adjusts $\delta_{\rm gf}(t)$, the grid-supporting unit can adjust its angle relative to $\delta_{\rm gf}(t)$. Fig. 6c shows the vector diagrams under this operating condition.

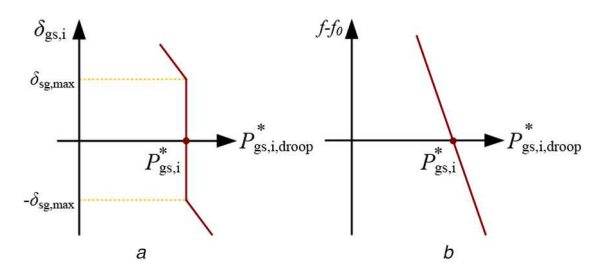


Fig. 7 Comparison of droop-based methods
(a) Proposed angle droop, (b) Conventional frequency droop

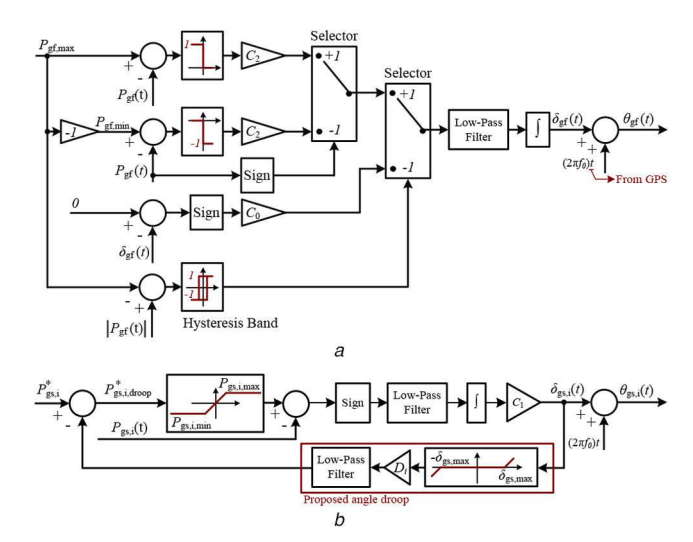


Fig. 8 Proposed real power sharing algorithm (a) Grid-forming unit, (b) Grid-supporting units

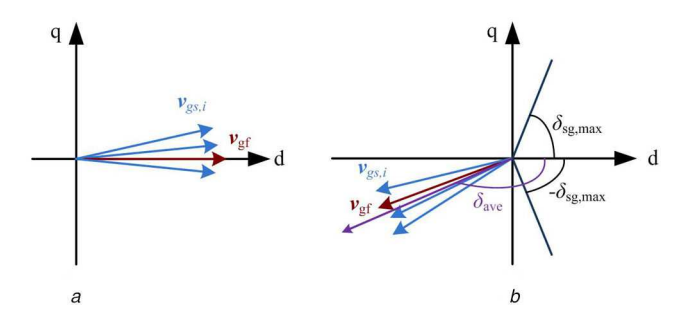


Fig. 9 Vector diagrams of the IBRs in the steady state when the grid-forming unit is

(a) Large (see text for definition), (b) Limited

3.3 Angle droop algorithm

To avoid the steady-state deviation of f_{sys} from f_0 , upper and lower trigger points for $\delta_{gs}(t)$ are defined. In our angle droop implementation, $|P_{gs}^*|$ is reduced when $\delta_{gs}(t)$ is outside these trigger points. The adjustment ΔP_{es}^* in (2) is calculated as

$$\Delta P_{\text{[gs]}}^* = \begin{cases} D(\delta_{\text{[gs],max}} - \delta_{\text{gs}}(t)), & \delta_{\text{[gs],max}} < \delta_{\text{gs}}(t) \\ D(\delta_{\text{[gs],min}} - \delta_{\text{gs}}(t)), & \delta_{\text{[gs],min}} > \delta_{\text{gs}}(t) \\ 0, & \text{otherwise,} \end{cases}$$
(6)

where D is the angle droop gain. With multiple grid-supporting units, D of each unit determines its power share.

Fig. 7 compares the droop characteristic of the proposed angle droop algorithm with the conventional frequency droop. The angle droop characteristic, Fig. 7a, has a soft limiter shape, while the frequency droop characteristic, Fig. 7b, is a straight sloped line. This is because in frequency droop all units are expected to operate at the same frequency but in angle droop units operate at different angles and a range of angles (as specified by $\delta_{(gs),min}$ and $\delta_{(gs),max}$ for each grid-supporting unit) is possible. For symmetry, in the remainder of this paper, it is assumed that $\delta_{(gs),min} = -\delta_{(gs),max}$ but

the proposed angle droop algorithm can operate without this assumption. The choice of $\delta_{\rm gs,max}$ is a trade-off between power sharing accuracy based on D coefficients and the time it takes to reach the steady state.

Fig. 8 shows the overall real power sharing algorithm generalised to multiple grid-supporting units. The hysteresis band prevents interference of the power limiting and angle control features of the grid-forming unit. A bandwidth too large allows $|P_{gf}(t)|$ to exceed $P_{gf,max}$, a bandwidth too small may result in system instability due to the frequent changes in the control mode. Therefore, the bandwidth should be chosen as a modest fraction of $P_{gf,max}$, e.g. 1%.

4 Parameter design and tuning

A discussion of some of the parameters, i.e. C_0 , C_1 , and $\delta_{\rm g,max}$, and hysteresis bands, is provided in the previous section. This section further discusses the parameters of the proposed algorithm and their design criteria.

4.1 Selection of ramp rates Ci

As mentioned above, the proposed algorithm ensures voltage angles are within their limits. However, since the ramp rates C_i to change angles are limited, it takes some finite time for the voltage vectors to rotate and reach the steady state. Without extra measures, the real powers of grid-supporting units are uncontrolled and may exceed their limits even though their reference values are limited. To prevent this, a variable gain is adopted: if the real power of a grid-supporting unit reaches its limit, the ramp rate is changed from C_1 to a larger value C_3 . If $C_3 > C_2$, the real power limiting scheme of the grid-forming unit can no longer change the real power of the grid-supporting unit as the voltage vector of the grid-supporting unit will rotate at the speed of $C_3 - C_2$. Therefore, the grid-supporting unit can limit its output real power during this time. Thus, the ramp rates should be

$$C_0 < C_1 < C_2 < C_3. (7)$$

4.2 Selection of droop parameters D_i , $\delta_{\rm gs,min}$, and $\delta_{\rm gs,max}$

This section discusses how the proposed angle droop algorithm determines the share of each grid-supporting unit in supplying $P_{\text{gs-total-change}}$ defined in Section 3.2. From (3) and (6)

$$P_{\text{gs-total-change}} = \sum \Delta P_{\text{gs,i}}^* = \sum D_i (\delta_{\text{gs,min}} - \delta_{\text{gs,i}}).$$
 (8)

If $P_{\text{gs-total-change}} = 0$, i.e. the grid-forming unit is large enough to supply the power demand beyond the preferred set points of the grid-supporting units, $\delta_{\text{gf}} = 0$ and all $v_{\text{gs,i}}$ vectors cluster around it as shown in Fig. 9a. Otherwise, as shown in Fig. 9b, voltage vectors are far from the zero angle and have an average angle of $\delta_{\text{ave}} = \text{mean}(\delta_{\text{gs,i}})$. If D_i values are small, $|\delta_{\text{ave}}|$ is large and for all grid-supporting units $\delta_{\text{gs,i}} \simeq \delta_{\text{ave}}$. Therefore

$$P_{\text{gs-total-change}} = \sum D_i (\delta_{\text{gs,min}} - \delta_{\text{ave}}). \tag{9}$$

Subsequently

$$\Delta P_{\rm gs,i}^* = \frac{D_i}{\sum D_i} P_{\rm gs-total-change} \,. \tag{10}$$

That is the real power change of each grid-supporting unit is proportional to its droop gain D_i . Choosing smaller D_i values results in more precise power sharing but a longer response time.

4.3 Selection of power limits

Power limits for grid-supporting units are based on their physical limits. For example, for renewable resources such as wind and PV, the maximum power is based on instantaneous maximum power point (MPP): $P_{\text{gs,max}}(t) < P_{\text{MPP}}(t)$; the minimum power is zero. For a

storage unit, the minimum and maximum power limits are based on the state of charge to avoid overcharge or over-discharge.

5 Performance evaluation

Several case studies are conducted to evaluate the performance of the proposed architecture. PSCAD/EMTDC is employed to model the fast electromagnetic transients of the inverters. Fig. 10 shows the study system chosen as the three-machine, IEEE/WSCC ninebus system.

The base values of the voltage and power used for per unit calculations are $230\,\mathrm{kV}$ and $100\,\mathrm{MVA}$. The rated powers of the IBRs at buses 1-3 are 250, 192, and $128\,\mathrm{MVA}$. Per unit currents

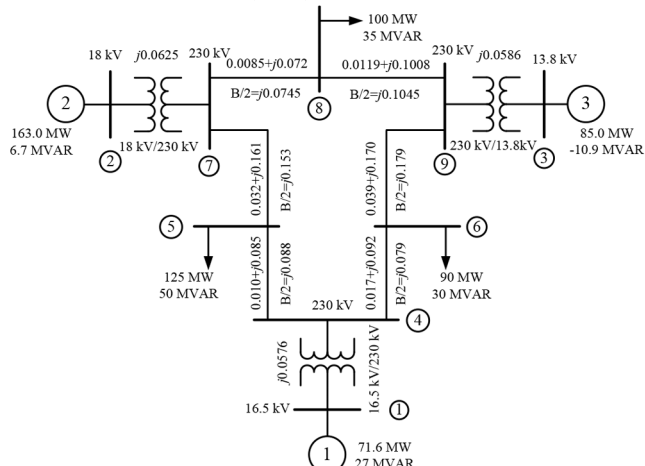


Fig. 10 IEEE/WSCC 9-bus study system

Table 2 Parameters of the controllers

voltage controller	$G_1 = 10, G_2 = 2$		
	$i_{t, i, \text{threshold}} = 1.5 \text{ pu } (i = 1, 2, 3)$		
real power controller	$C_0 = 0.75, C_1 = 1.00$		
	$C_2 = 1.25, C_3 = 5.00$		
	$P_{\rm gs,1,max} = 250 \text{MW}, P_{\rm gs,3,max} = 128 \text{MW}$		
	$P_{\rm gf,max} = 192 MW$		
angle droop	$D_1 = 5.0 \times 10^3 \text{MW/rad}, D_3 = 2.5 \times 10^3 \text{MW/rad}$		
	$\delta_{ m gs,max} = - \delta_{ m gs,min} = 0.75 m rad$		

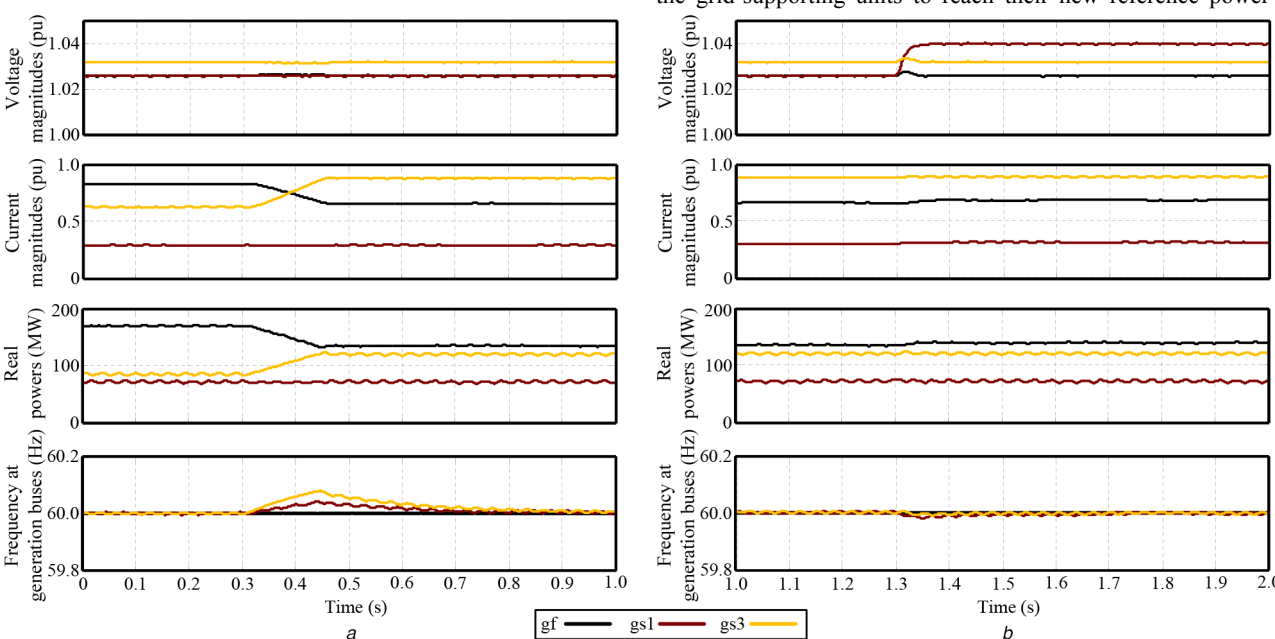


Fig. 11 Case study 5.1: measurements as (a) $P_{gs,1}^*$ changes from 85 to 120 MW at t = 0.3 s, (b) $|v_{gs,1}^*|$ changes from 1.026 to 1.040 pu at t = 1.3 s

are calculated on the base of their associated generator. The loads are modelled as a constant impedance calculated at the nominal voltage, except in Section 5.4, where induction motor loads are used. All three IBRs are interfaced to the grid via an inverter. The IBR at bus 2 is chosen as the grid-forming unit (gf), and the IBRs at buses 1 and 3 are chosen as grid-supporting units (gs1 and gs3). Initially, buses 1–3 regulate their output real power and bus voltage magnitudes to the rated values of the nine-bus system. Table 2 shows the controller parameters.

5.1 Step change in $P_{\rm gs,i}^*$ and $|v_{\rm gs,i}^*|$

In this case, initially the grid-supporting units output their preferred real powers. At t=0.3 s, $P_{\rm gs,3}^*$ increases in a step by 35 MW, and at t=1.3 s, $|v_{\rm gs,1}^*|$ increases in a step by 0.014 pu. The loads do not change.

Fig. 11 shows voltage, current, real power, and frequency at buses 1–3. As Fig. 11 shows, $P_{\rm gs,3}(t)$ tracks its set point $P_{\rm gs,3}^*$ with a rise time of 150 ms (inversely proportional to C_1) and $|v_{\rm gs,1}(t)|$ tracks $|v_{\rm gs,1}^*|$ with a rise time of 50 ms, and since $|i_{\rm t,}i(t)| < |i_{\rm t,}i|_{\rm threshold}$, the voltage controller tracks its set-point value with the gain of G_1 . During transients, the current magnitudes change smoothly. Since the load is unchanged, after the increase in $P_{\rm gs,3}(t)$, $P_{\rm gf}(t)$ decreases with a gain of C_2 to maintain power balance. When there is a step change in $P_{\rm gs,3}^*$, the proposed angle-droop algorithm is activated, and the frequency returns to its rated value (60 Hz) in the steady state.

5.2 Load increase

In this case, initially, the grid-supporting units output their preferred real powers. At t=1 s, the real power of the load at bus 6 increases by 15 MW, and at t=3 s, the real power of the load at bus 5 increases by 80 MW. This scenario is simulated once assuming the grid-forming unit can accommodate the whole load change ($P_{\rm gf,max}$ is large) and once when it cannot. As Fig. 12 shows, in both cases, the first load increase is supported by an increase in $P_{\rm gf}(t)$ with the gain of C_2 because $|P_{\rm gf}(t)| < P_{\rm gf,max}$. However, the two systems respond differently to the second load increase. In the system with the large grid-forming unit, the load increase is supported by an increase in $P_{\rm gf}(t)$ and in the steady state, $P_{\rm gf}=264$ MW. In the system with the small grid-forming unit, the load increase is initially responded to by an increase in $P_{\rm gf}(t)$ until $P_{\rm gf}(t) = P_{\rm gf,max}$. Then, $P_{\rm gs,l}(t)$ and $P_{\rm gs,3}(t)$ ramp up. It takes ~1.5 s for the grid-supporting units to reach their new reference power set

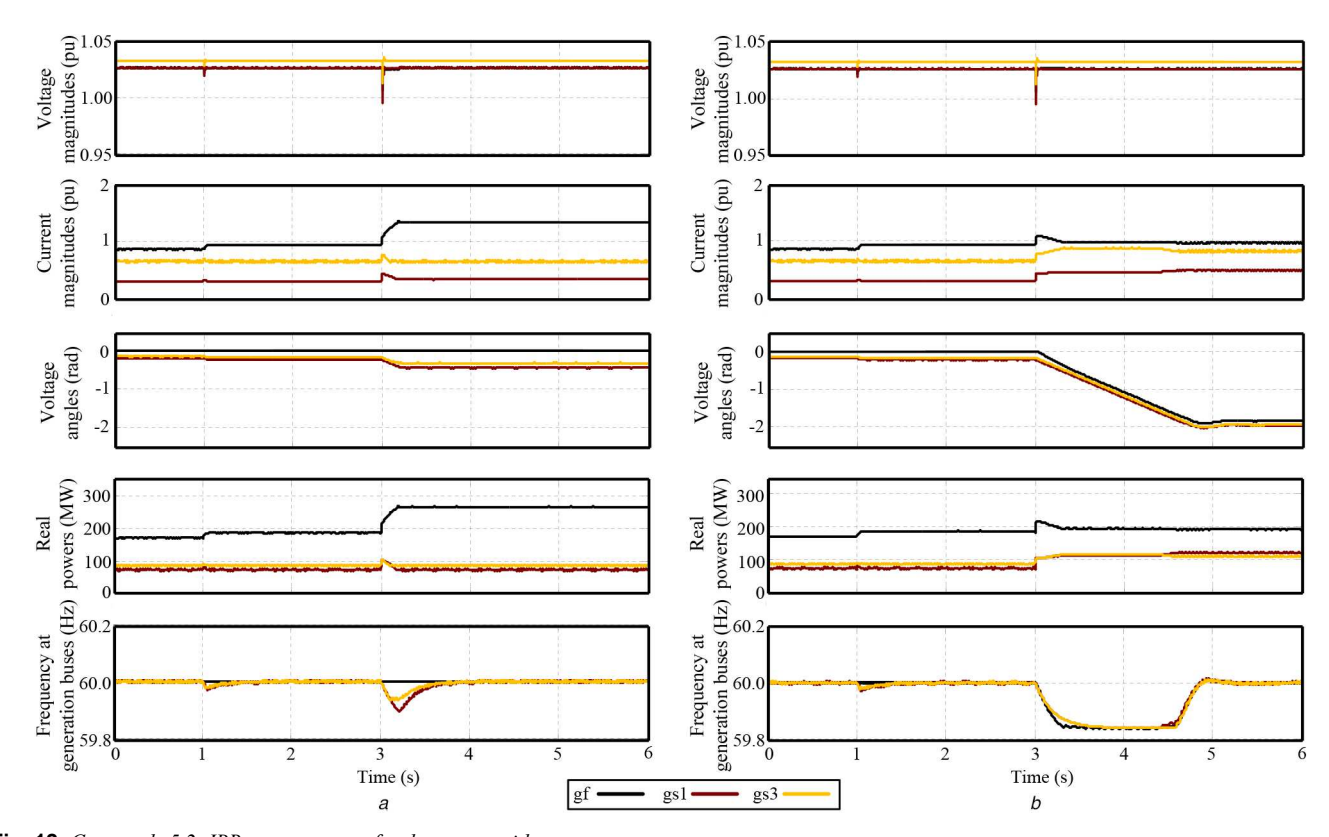


Fig. 12 Case study 5.2: IBR measurements for the system with a (a) Large (compared with load demand) grid-forming unit, (b) Small grid-forming unit. In both systems, the load at bus 6 increases by 15 MW at t = 1 s and the load at bus 5 increases by 80 MW at t = 3 s

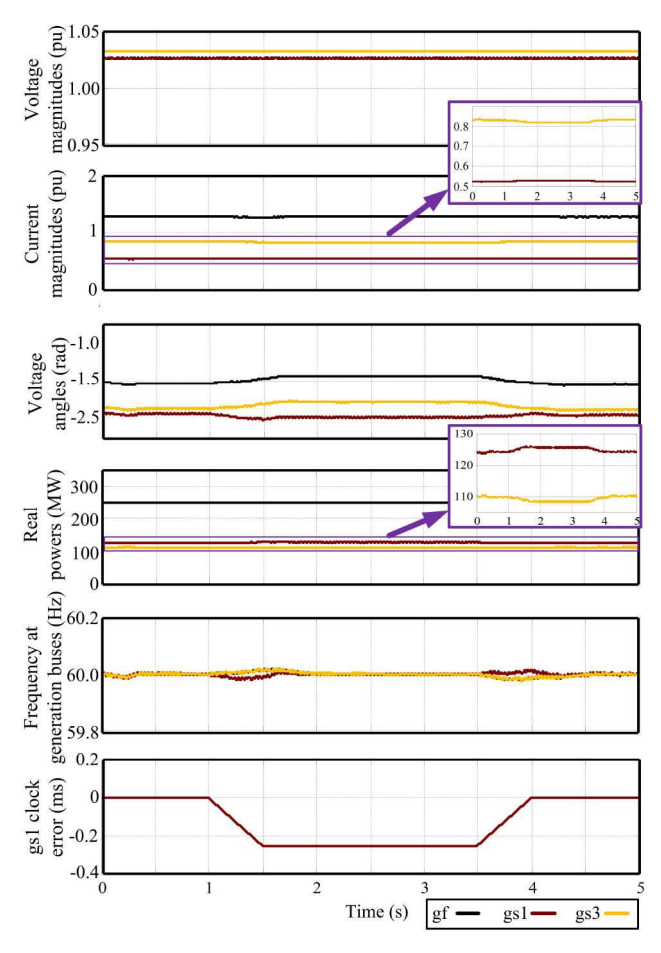


Fig. 13 Cases study 5.3: the performance of the system when the GPS signal is not available for 0.5 s

points. During this time, $P_{gs,1}(t)$ and $P_{gs,3}(t)$ are not under control but are within their limits. In the steady state, $\Delta P_{gs,1}^* = 48 \text{ MW}$ and $\Delta P_{gs,3}^* = 23 \text{ MW}$. The ratio $\Delta P_{gs,1}^* / \Delta P_{gs,3}^*$ is 2.09, which is very close to $D_1/D_3 = 2.00$ (4.5% error). In summary, when the system has a small grid-forming unit, once it reaches $P_{gf,max}$, the proposed angle droop algorithm is activated to return the system frequency to 60 Hz. The voltage controller can return the voltage magnitudes to their set point values in both cases, which confirms the performance of the proposed controllers.

5.3 Loss of GPS signal

This case study investigates the effects of temporary loss of GPS signals and potential subsequent tracking error of time. Initially, the system runs as in the last scenario of Section 5.2. At t = 1 s, the grid-supporting unit 1 (gs,1) loses its GPS signal and exclusively uses its internal clock. It is assumed that in the first 0.5 s the internal clock linearly deviates from the actual time and after that the error remains constant (-0.25 ms). It should be noted that this case study considers an exaggerated case. Local clocks are expected to have a much better performance. Fig. 13 shows the results. As the result of time tracking error, $\Delta P_{\rm gs,1}^*$ changes from 48 to 50 MW and $\Delta P_{\rm gs,3}^*$ changes from 23 to 21.8 MW. Therefore, the ratio $\Delta P_{\rm gs,1}^*/\Delta P_{\rm gs,3}^*$ changes from 2.09 to 2.29 (an additional 9.56% error in power sharing). At t = 4 s, gs,1 regains access to GPS signal and synchronises its internal clock with the GPS time in 0.5 s. This synchronisation brings $\Delta P_{\rm gs,1}^*$ and $\Delta P_{\rm gs,3}^*$ back to 48 and 23 MW, respectively. This temporary loss of the GPS signal slightly degrades the accuracy of power sharing, but the controller can regain its performance even in this exaggerated case.

5.4 Dynamic loads

This case study investigates the performance of the proposed algorithm in the presence of dynamic loads with inertia. Two induction motors (IMs) are connected to bus 6 (15 MW, IM1) and bus 5 (80 MW, IM2). Initially, both IMs run under no-load conditions. IM1 is loaded at t = 1 s and IM2 is loaded at t = 3 s.

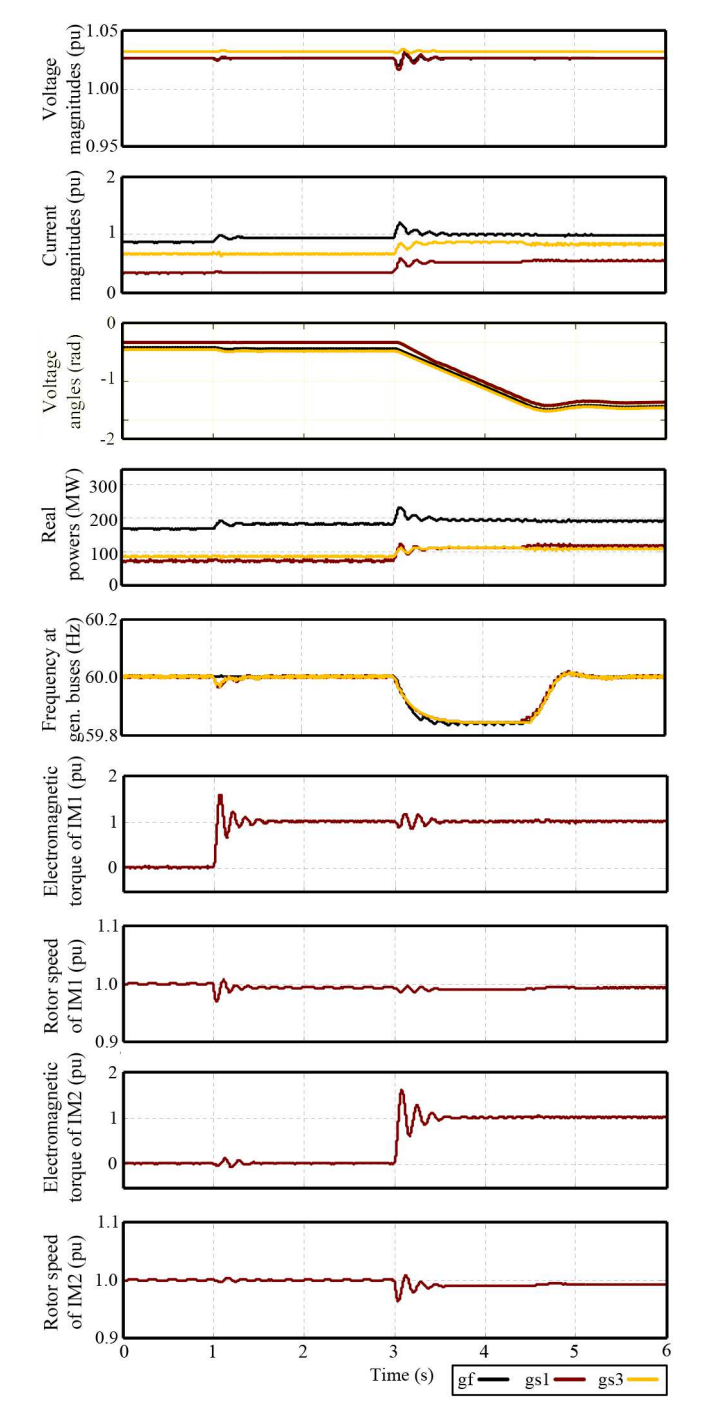


Fig. 14 Case study 5.4: measurements of buses I-3 and machine loads as IM1 changes from no-load to full-load at t=1 s and IM2 changes from no-load to full-load at t=3 s

Both loads are linear with a mechanical torque proportional to speed. Fig. 14 shows the results. The grid-forming unit provides all of the power needed by IM1 since its power is smaller than $P_{\rm gf,max}$ and it ramps up with the gain of C_2 . However, loading of IM2 needs power from the grid-supporting unit and hence, results in increase of $P_{\rm gs,l}(t)$ and $P_{\rm gs,3}(t)$ based on their droop gains D_1 and D_3 , respectively. When IM2 is loaded, there is a drop in the system frequency; however, the proposed angle-droop is activated during this time and it returns the frequency to 60 Hz. During start-up, the rotor speeds are smooth, but their electromagnetic torques oscillate. Subsequently, their real powers (electromagnetic torque times rotor speed) oscillate too, resulting in small oscillations in the voltage and real power. These oscillations are related to the mechanical modes of the IMs and their analysis is beyond the scope of this paper.

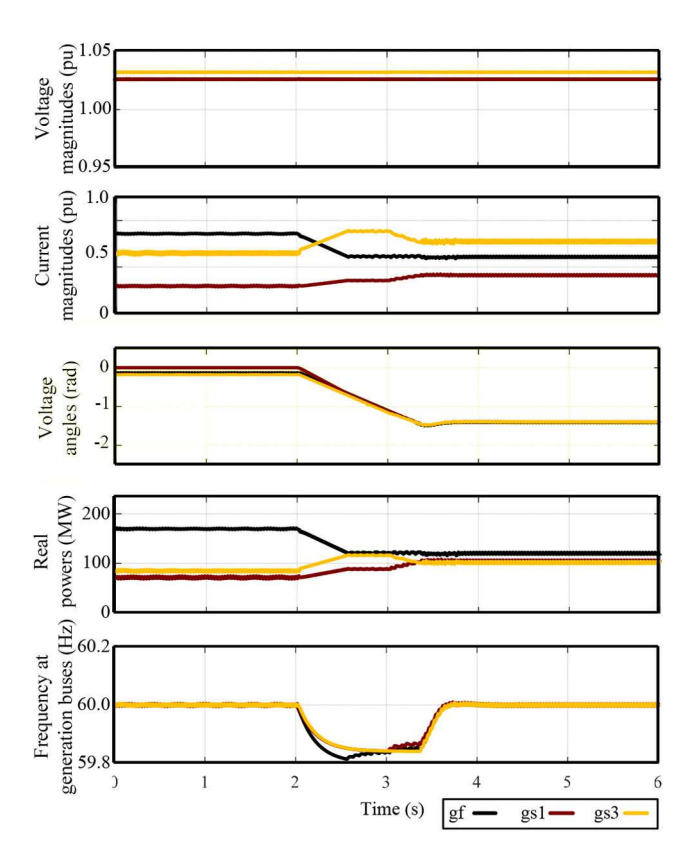


Fig. 15 Case study 5.5: measurements at buses 1–3 when $P_{\rm gf,max}$ decreases from 192 to 120 MW at t=2 s

5.5 Power redispatch

This case study evaluates the performance of the proposed angle-droop algorithm and controller to track a change in $P_{\rm gf,max}$. In this case study, initially, the grid-supporting units output their preferred real powers and the grid-forming unit provides 170 MW. At $t=2\,\rm s$, $P_{\rm gf,max}$ decreases from 192 to 120 MW. Subsequently, a portion of the load initially supplied by the grid-forming unit has to be provided by the grid-supporting units. Fig. 15 shows that after the reduction in $P_{\rm gf,max}$, $P_{\rm gs,1}$ and $P_{\rm gs,3}$ increase by 33 and 17 MW to compensate for the mismatch between generation and demand. This change is proportional to the droop gains of the grid-supporting units as expected. As Fig. 15 shows, when there is a decrease in $P_{\rm gf,max}$, the frequency drops; however, the proposed algorithm actives and returns system frequency to the rated value of 60 Hz.

5.6 Fault

This case study evaluates the system response to a fault. Initially, the system operates under nominal conditions when a three-phase bolted fault occurs at $t=0.2\,\mathrm{s}$ in the middle of one of the double transmission lines between buses 4 and 5 (this second line is added for this case study). After 100 ms, the fault is cleared by the circuit breakers at the two ends of the line. As Fig. 16a shows, the current limiting function of the controller activates when the current reaches the threshold value (Table 2). This threshold depends on the rating of the switches (with respect to the inverter rating), cooling mechanism, and system considerations. In this paper, this limit is chosen heuristically. The limiter is not a replacement for protection or the current limitation provided by limiting the reference current values.

The maximum instantaneous current magnitude is 1.8 pu. Moreover, minimum and maximum voltage amplitudes of the generation buses are 0.2 and 1.1 pu, respectively. When the fault is cleared, the system returns to its normal operation. Fig. 16b shows the result of the same case study if the proposed voltage controller is not augmented with a current limiter. The maximum current is 4.8 pu and the minimum and maximum voltages are 0.5 and 2.0 pu.

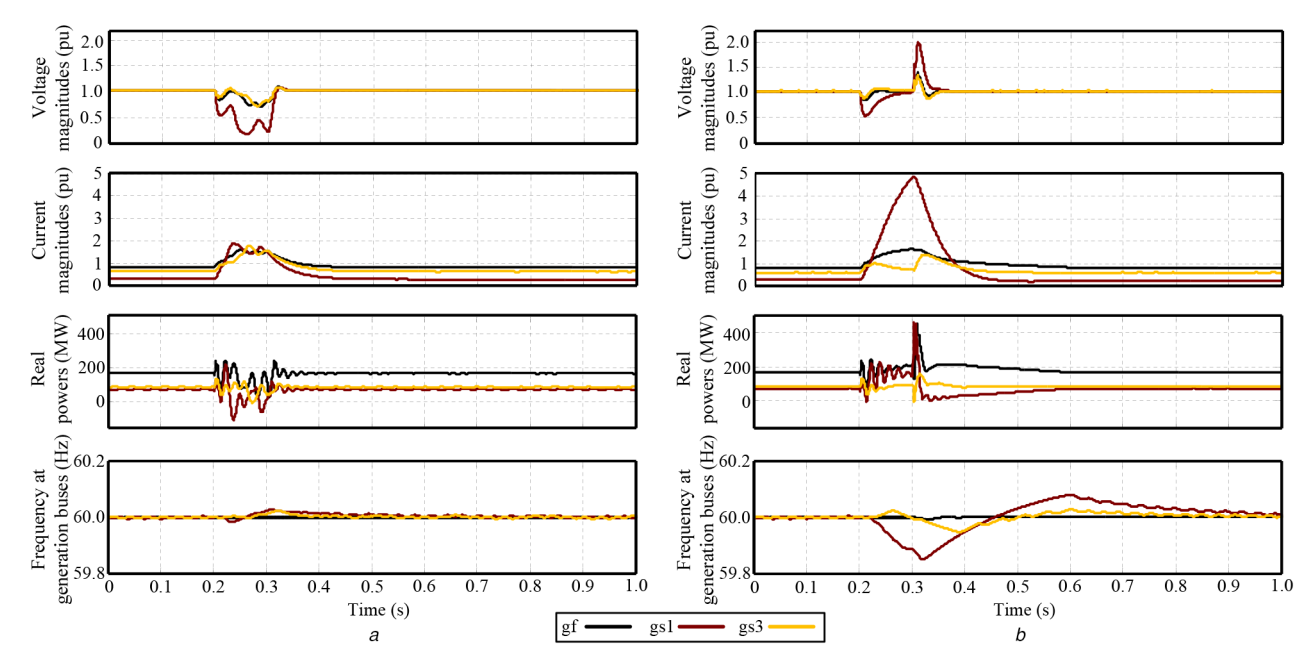


Fig. 16 Case study 5.6: measurements at buses I-3 when a fault occurs at t=0.2 s and clears after 100 ms (a) With the current limiter, (b) Without the current limiter

Conclusion

This paper proposes a new angle-droop-based algorithm for power sharing of generation resources in a 100% inverter-based power system. The proposed method only utilises GPS and local signals and does not need central coordination or communication. The proposed algorithm considers the current and real power limits of inverters during both steady-state and transient operations and respects their preferred set points as much as possible. A parametric design guideline is also proposed for the proposed control and power sharing methods. Simulation results confirm the effectiveness of the proposed algorithm in different scenarios change including load (the droop ratio error < DIFadd ><< /DIFadd > 5%), energisation of dynamic loads, power redispatch, and fault. A suggested future work, which reinforces the proposed algorithm, is the stability analysis of the power system with the proposed controller and angle droop-based power-sharing method.

7 References

- [1] Kroposki, B., Johnson, B., Zhang, Y., et al.: 'Achieving a 100% renewable grid: operating electric power systems with extremely high levels of variable renewable energy', IEEE Power Energy Mag., 2017, 15, (2), pp. 61-73
- Halley, A., Martins, N., Gomes, P., et al.: 'Effects of increasing power [2] electronics based technology on power system stability: performance and operations', *CIGRE Sci. Eng.*, 2018, **11**, (2), pp. 5–17 Zhang, Y., Bank, J., Muljadi, E., *et al.*: 'Power system infrastructure: do we
- [3] face a complete power-electronics-based power system and energy-storage infrastructure?', IEEE Power Electron. Mag., 2016, 3, (2), pp. 42-45
- [4] 'Variable energy resource modeling workshop, North America Cooperation', 2017. Available at http://www.nerc.com/comm/pc/pages/powerplant-modeling-and-verification-task- force.aspx
- Eftekharnejad, S., Vittal, V., Heydt, G.T., et al.: 'Impact of increased [5] penetration of photovoltaic generation on power systems', IEEE Trans. Power Syst., 2013, **28**, (2), pp. 893–901
- Zhang, Y., Bank, J., Muljadi, E., et al.: 'Angle instability detection in power [6]
- Systems with high-wind penetration using synchrophasor measurements', *IEEE J. Emerging Sel. Top. Power Electron.*, 2013, **1**, (4), pp. 306–314 Rocabert, J., Luna, A., Blaabjerg, F., *et al.*: 'Control of power converters in AC microgrids', *IEEE Trans. Power Electron.*, 2012, **27**, (11), pp. 4734–4749 [7]
- Olivares, D., Mehrizi-Sani, A., Etemadi, A., et al.: 'Trends in microgrid [8] control', IEEE Trans. Smart Grid, 2014, 5, (4), pp. 1905-1919
- Yazdanian, M., Mehrizi-Sani, A.: 'Distributed control techniques in microgrids', *IEEE Trans. Smart Grid*, 2014, **5**, (6), pp. 2901–2909 [9]
- [10] Xu, Y.: 'Robust finite-time control for autonomous operation of an inverter-based microgrid', *IEEE Trans. Ind. Inf.*, 2017, **13**, (5), pp. 2717–2725

- Mousavi, M., Teymouri, A., Shabestari, P.M., et al.: 'Performance evaluation of an angle droop-based power sharing for a power system dominated by inverter-based generation. 45th Annual Conf. of the IEEE Industrial Electronics Society (IECON 2019), Lisbon, Portugal, 2019, vol. 1, pp. 2464–
- [12] Zhong, Q.C., Weiss, G.: 'Synchronverters: inverters that mimic synchronous generators', IEEE Trans. Ind. Electron., 2011, 58, (4), pp. 1259-126
- [13] Arani, M.F.M., El-Saadany, E.F.: 'Implementing virtual inertia in DFIG-based wind power generation', IEEE Trans Power Syst, 2013, 28, (2), pp. 1373-1384
- Ramasubramanian, D., Vittal, V., Undrill, J.M.: 'Transient stability analysis of [14] an all converter interfaced generation WECC system'. Power Systems Computation Conf. (PSCC), Genoa, Italy, 2016, pp. 1–7
 Denis, G., Prevost, T., Debry, M., et al.: 'The migrate project: the challenges
- of operating a transmission grid with only inverter-based generation. A gridforming control improvement with transient current-limiting control', IET Renew. Power Gener., 2018, 12, (5), pp. 523–529 Yazdanian, M., Mehrizi-Sani, A.: 'Washout filter-based power sharing', IEEE
- [16] Trans. Smart Grid, 2016, 7, (2), pp. 967-968
- Ramasubramanian, D., Farantatos, E., Ziaeinejad, S., et al.: 'Operation paradigm of an all converter interfaced generation bulk power system', IET Gener. Transm. Distrib., 2018, 12, (19), pp. 4240-4248
- [18] Kolluri, R.R., Mareels, I., Alpcan, T., et al.: 'Power sharing in angle droop controlled microgrids', IEEE Trans. Power Syst., 2017, 32, (6), pp. 4743-
- [19] Moussa, H., Shahin, A., Martin, J.P., et al.: 'Optimal angle droop for power sharing enhancement with stability improvement in islanded microgrids', IEEE Trans. Smart Grid, 2018, 9, (5), pp. 5014-5026
- [20] John, B., Ghosh, A., Zare, F.: 'Load sharing in medium voltage islanded microgrids with advanced angle droop control', IEEE Trans. Smart Grid, 2018, **9**, (6) pp. 6461–6469
- [21] Moussa, H., Shahin, A., Martin, J., et al.: 'Optimal angle droop for power sharing enhancement with stability improvement in islanded microgrids', IEEE Trans. Smart Grid, 2018, 9, (5), pp. 5014-5026
- Kahrobaeian, A., Mohamed, Y.A.R.I.: 'Networked-based hybrid distributed power sharing and control for islanded microgrid systems', *IEEE Trans. Power Electron.*, 2015, **30**, (2), pp. 603–617
- Majumder, R., Ledwich, G., Ghosh, A., et al.: 'Droop control of converterinterfaced microsources in rural distributed generation', IEEE Trans. Power Deliv., 2010, 25, (4), pp. 2768-2778
- 'Program on technology innovation: grid operation with 100% inverterinterfaced supply resources – interim report', 2018. Available at https://www.epri.com/pages/product/3002012298/
- Holbert, K.E., Heydt, G.I., Ni, H.: 'Use of satellite technologies for power system measurements, command, and control', Proc. IEEE, 2005, 93, (5), pp.
- Etemadi, A.H., Davison, E.J., Iravani, R.: 'A generalized decentralized robust control of islanded microgrids', IEEE Trans. Power Syst., 2014, 29, (6), pp. 3102-3113